

REPORT DOCUMENTATION PAGE

Form Approved
OMB No. 0704-0188

Public reporting burden for this collection of information is estimated to average 1 hour per response, including the time for reviewing instructions, searching existing data sources, gathering and maintaining the data needed, and completing and reviewing this collection of information. Send comments regarding this burden estimate or any other aspect of this collection of information, including suggestions for reducing this burden to Department of Defense, Washington Headquarters Services, Directorate for Information Operations and Reports (0704-0188), 1215 Jefferson Davis Highway, Suite 1204, Arlington, VA 22202-4302. Respondents should be aware that notwithstanding any other provision of law, no person shall be subject to any penalty for failing to comply with a collection of information if it does not display a currently valid OMB control number. **PLEASE DO NOT RETURN YOUR FORM TO THE ABOVE ADDRESS.**

1. REPORT DATE (DD-MM-YYYY) 29-05-2009		2. REPORT TYPE Technical Paper		3. DATES COVERED (From - To)	
4. TITLE AND SUBTITLE First-Principles Monte-Carlo Simulation of Homogeneous Condensation in Atomic and Molecular Plumes				5a. CONTRACT NUMBER	
				5b. GRANT NUMBER	
				5c. PROGRAM ELEMENT NUMBER	
6. AUTHOR(S) Ryan Jansen (USC); Sergey Gimelshein, & Michael Zeifman (ERC); Ingrid Wysong (AFRL/RZSA)				5d. PROJECT NUMBER	
				5f. WORK UNIT NUMBER 23080532	
7. PERFORMING ORGANIZATION NAME(S) AND ADDRESS(ES) Air Force Research Laboratory (AFMC) AFRL/RZSA 10 E. Saturn Blvd. Edwards AFB CA 93524-7680				8. PERFORMING ORGANIZATION REPORT NUMBER AFRL-RZ-ED-TP-2009-219	
9. SPONSORING / MONITORING AGENCY NAME(S) AND ADDRESS(ES) Air Force Research Laboratory (AFMC) AFRL/RZS 5 Pollux Drive Edwards AFB CA 93524-7048				10. SPONSOR/MONITOR'S ACRONYM(S)	
				11. SPONSOR/MONITOR'S NUMBER(S) AFRL-RZ-ED-TP-2009-219	
12. DISTRIBUTION / AVAILABILITY STATEMENT Approved for public release; distribution unlimited (PA #09220).					
13. SUPPLEMENTARY NOTES For presentation at the 41 st AIAA Thermophysics Conference, San Antonio, TX, 22-25 June 2009.					
14. ABSTRACT First-principles kinetic theory is used in this work to analyze non-equilibrium homogeneous condensation of argon and water. The present model uses a recombination-reaction energy-dependent mechanism of the DSMC method for the dimer formation, and RRK model for the evaporation. Three-step validation of the model is conducted, (i) comparison of clusterization rates in an equilibrium heat bath with theoretical predictions, (ii) comparison of the argon dimer fractions in an orifice expansion with semi-analytical correlations, and (iii) comparison of water cluster size distributions with experimental measurements. Reasonable agreement was observed for all three parts of the validation.					
15. SUBJECT TERMS					
16. SECURITY CLASSIFICATION OF:			17. LIMITATION OF ABSTRACT	18. NUMBER OF PAGES	19a. NAME OF RESPONSIBLE PERSON
a. REPORT	b. ABSTRACT	c. THIS PAGE			Dr. Ingrid Wysong
Unclassified	Unclassified	Unclassified	SAR	17	19b. TELEPHONE NUMBER (include area code) N/A

First-Principles Monte-Carlo Simulation of Homogeneous Condensation in Atomic and Molecular Plumes

Ryan Jansen*

University of Southern California, Los Angeles, CA 90089

Sergey Gimelshein[†] and Michael Zeifman[†]

ERC, Inc., Edwards AFB, CA 93524

Ingrid Wysong[‡]

Air Force Research Laboratory, Edwards AFB, CA 93524

First-principles kinetic theory is used in this work to analyze non-equilibrium homogeneous condensation of argon and water. The present model uses a recombination-reaction energy-dependent mechanism of the DSMC method for the dimer formation, and RRK model for the evaporation. Three-step validation of the model is conducted, (i) comparison of clusterization rates in an equilibrium heat bath with theoretical predictions, (ii) comparison of the argon dimer fractions in an orifice expansion with semi-analytical correlations, and (iii) comparison of water cluster size distributions with experimental measurements. Reasonable agreement was observed for all three parts of the validation.

I. Introduction

Two different approaches for modeling the condensation in rapidly expanding plumes have been reported in the literature. The first approach, known as the classical approach, takes its starting point from the classical nucleation theory (CNT) which is based on equilibrium thermodynamics.^{1,2} The second one, known as the kinetic approach, treats nucleation as the process of kinetic chemical aggregation.³

The classical approach considers the energy of cluster formation from the vapor state. Assuming unimolecular reactions of cluster growth and decay, CNT calculates the corresponding condensation and evaporation rates using the Gibbs distributions and the principle of detailed balance.³⁻⁶ The nucleation rate is then calculated assuming a steady state condition.⁷ Although a rapidly expanding supersonic plume is quite different from the isothermal, ideal gas environment assumed by CNT, the classical predictions were found to be qualitatively correct for the modeling of cluster formation in supersonic jets.⁸⁻¹² There are many examples, however, when CNT-based results cannot be fitted to experimental data. The CNT-based prediction of the cluster size distributions¹³ significantly deviated from experimental data.¹⁴ This is consistent with the work of Ref. 15, where it was also found that the correct prediction of the cluster size distribution along with the internal and translational energy distributions is beyond the area of applicability of the classical approach.

The reasons for the discrepancy between the CNT-based distributions and experimental data are both due to problems inherent in CNT and the flow conditions of expanding plumes. The former include the ambiguous definition of the surface energy of small clusters,⁷ the negligence of the rotational and translational degrees of freedom of freshly nucleated clusters,¹⁶ and the unrealistic description of vapor-cluster and cluster-cluster interactions.¹² The latter are related to the main assumptions underlying the derivation of the nucleation

*Undergraduate Student, Astronautical Engineering

[†]Consultant

[‡]Branch Chief, Propulsion Directorate

Copyright © 2009 by the authors. Published by the American Institute of Aeronautics and Astronautics, Inc. with permission.

rate, which may be violated in rapidly expanding supersonic flows.¹⁷ The transient time needed for a system to reach steady state in terms of the unimolecular cluster reactions may be such that the jet macroparameters will significantly change during that time. Moreover, many theoretical and experimental results^{18–20} suggest that local thermal equilibrium does not exist in an expanding supersonic jet. Thus the process of cluster formation is not likely to be isothermal. There have been recent advances in CNT mainly aimed at achieving a more realistic model for condensation and evaporation rates,^{6,16,21–24} but other principal deficiencies of CNT and its application to the non-equilibrium environment still have yet to be addressed. Note that despite these deficiencies, the steady state CNT nucleation rate with a correction⁶ is used in such commercial fluid dynamics codes as GASP or CFD-particle.

Unlike CNT, the kinetic approach does not assume local thermodynamic equilibrium. Instead, a microscopic view of the interactions of monomers and clusters is established either analytically via a mathematical model, e.g., by the Smoluchowski equations where the interaction between particles is modeled by the reaction rates,^{25–27} or in computer simulations, e.g., in molecular dynamics (MD) calculations where the interaction is modeled by an interaction potential.^{28–30} It can be shown that the application of the Smoluchowski equations to the modeling of clustering in supersonic jets is computationally unfeasible. Even though MD simulations might seem attractive (since no information besides the interaction potential is needed to perform the calculations), they are computationally limited to a system size of about one million gas particles and a time scale of a few nanoseconds at most. In real plumes, either thruster nozzle or ablation originated, the number of gas particles and the expansion time is greater by many orders of magnitude (see, for example,^{9,31}). Therefore, the MD technique cannot be directly applied to the simulation of even small laboratory-sized supersonic jets.

A promising direction in modeling the coupled condensation flow is the use of a kinetic particle simulation method, direct simulation Monte Carlo (DSMC),³² which is applicable in a wide range of flow regimes from free molecular to near continuum. It is a statistical approach for solving the spatially nonuniform master Leontovich equation for the N-particle distribution function and, in the limit of a large N, it represents an accurate solution of the Boltzmann equation. The advantage of DSMC as compared to other methods is that complicated cluster-cluster and cluster-monomer interactions including the multi-body reactions of cluster nucleation can be seamlessly incorporated.

The DSMC method has been used to study the process of cluster formation and evolution for a number of years.^{5,33,34} However, the gas flow in the earlier studies was uniform, the considered cluster size range was very narrow (up to 25 monomers in a cluster) and the examined reaction types were unrealistically limited to elastic collisions, cluster and monomer sticking to clusters, and evaporation of monomers from clusters.

More recently, the DSMC method has been extensively and successfully applied to modeling the processes of cluster formation and evolution in supersonic jets by Levin et al (see, for example, Refs. 12, 35, 36). The model initially was based on the classical nucleation theory, with the new clusters being formed at the critical size. Further work of these authors³⁷ extended the kinetic dimer formation approach of Ref. 38, who assumed that a ternary collision always results in a dimer formation, to include molecular dynamic (MD) simulations for obtaining information on the probability of dimer formation in such ternary collisions. The work³⁹ used a temperature-dependent probability of formation of argon dimers.

Although the use of MD has a number of advantages, due to its inherent limitations, the obtained probability cannot be unambiguously related to such characteristics of the ternary collision as the internal energy of the collision complex and the kinetic energy of the impinging monomer. Another possible limitation of the above work is that even though the nucleation process is fully kinetic in the most recent papers, they the CNT rate is used for evaporation, although there may be more sophisticated models for nonequilibrium cluster physics.⁴⁰

In the present paper, the DSMC approach for modeling of homogeneous nucleation in rapidly expanding plumes is extended to include a number of new features. Most importantly, a truly kinetic RRK model⁴¹ is implemented to characterize the cluster evaporation rates. Then, an energy dependent collision procedure similar to the recombination reaction model of Ref. 42 is used for the collision complex formation. An empirical parameter is used for the inelastic collision number in the cluster-monomer collisions. For dimers, this parameter was calibrated through the comparison of the computed nucleation rates and equilibrium constants in thermal bath with available theoretical and experimental data for argon and water. Additional validation analysis is conducted through comparison with the empirical correlation⁴³ for argon and measurements of cluster size distribution in water expansions.⁴⁴

II. Computational model of homogeneous nucleation

In the present first-principle model of homogeneous condensation formulated for the DSMC method, all of the most important processes of cluster nucleation and evolution are considered at the microscopic level. The main processes that are included in the model and described in detail below are (i) formation of collision complexes through the binary collisions of cluster-forming monomer species, (ii) creation of dimers through the collision stabilization of collision complexes, (iii) elastic monomer-cluster collisions that change the translational and internal energies of colliding particles, (iv) inelastic monomer-cluster collisions that result in monomer sticking, (v) cluster-cluster coalescence, (vi) evaporation of monomers from clusters. The details on each of these processes are given below.

A. Collision complex formation and stabilization

One of the important assumptions of the present model is that all pairs of colliding particles create collision complexes. A collision complex is a pair of monomers that have collided, and may have the conditions necessary to form a dimer if struck by a third particle during its lifetime. The collision complex lifetime, t_l , is assumed to be dependent on the type of monomers and their relative collision velocity, with the functional dependence given by the well known Bunker's expression⁴⁵

$$t_l = 1.5\sigma_0\mu^{\frac{1}{2}}\epsilon_0^{\frac{1}{6}}E^{-\frac{2}{3}}, \quad (1)$$

where σ_0 and ϵ_0 are the potential depth and separation distance parameters of the Lennard-Jones potential, μ is the reduced mass of the colliding particles, and E is their relative translational energy. The values of σ_0 and ϵ_0 used in this work are 3.166×10^{-10} m and 1.079×10^{-21} J for water, and 3.405×10^{-10} m and 1.654×10^{-21} J for argon.

The process of interaction of collision complexes with surrounding gas particles is modeled using the majorant frequency scheme⁴⁶ with the assumption that the collision complex – third particle interactions are governed by the Variable Hard Sphere (VHS) interaction model.⁴⁷ The VHS parameters of a collision complex were assumed to be those of the comprising monomers.

Generally, the probability $P(\tau)$ that a collision complex will collide with a third particle during an arbitrary time τ is

$$\frac{dP(\tau)}{d\tau} = \nu(1 - P(\tau)) \quad (2)$$

where ν is the collision frequency of the collision complex with third particles. For a mixture of N_s gas species, ν is expressed as

$$\nu = \sum_{i=1}^{N_s} n_i \langle \sigma g \rangle, \quad (3)$$

where σ is the corresponding total collision cross-section, g is the relative collision velocity between particles, and brackets denote averaging over g . Obviously, the probability that the collision complex will move freely and not collide during τ is given by

$$P_{free}(\tau) = e^{(-\tau\nu)}. \quad (4)$$

This expression represents the probability that no dimer will be formed during τ . Using the inverse transform,

$$\tau_c = -\ln(R/\nu), \quad (5)$$

where R is a random number uniformly distributed between 0 and 1. The majorant frequency algorithm for each pair of colliding monomers is therefore as follows.

1. Calculate t_l and $\nu_{majorant}$ and set $t_0 = 0$, $i = 1$. Here, $\nu_{majorant} = n\overline{\sigma_{max}g_{max}}$ is the majorant collision frequency, and σ_{max} and g_{max} are maximum cross section and relative collision velocity, respectively.
2. Calculate

$$t_i = t_{i-1} - \ln\left(\frac{R}{\nu_{majorant}}\right) \quad (6)$$

3. If $t_i > \Delta t$, where Δt is the simulation timestep, go to the the next pair of monomers.
4. If $t_i < \Delta t$, then a physical collision occurs with a probability $P_c = \frac{\nu(g)}{\sigma g} \sigma_{max} g_{max}$. With a probability $1 - P_c$, $i = i + 1$ and the algorithm returns to step 2.

In this algorithm, for consistency with the collision complex lifetime determination, an expression for the diameter d of the collision complex recommended in Ref. 45 was used,

$$d = 3^{\frac{1}{2}} \sigma_0 (\epsilon_0 / E)^{\frac{1}{6}}. \quad (7)$$

B. Dimer stabilization

If there is a physical collision between a collision complex and a third particle, there is a possibility of forming a stable dimer as a result of such a collision. Generally, the probability of the formation of a stable dimer (dimer stabilization) depends on the colliding species and the energies - both translational and internal - of the colliding particles. In this work, constant stabilization probabilities of 0.2 for Ar³⁷ and 1.0 for H₂O were assumed, which seem reasonable for the range of temperatures under consideration.

Dimer creation through the collisional stabilization of collision complexes is a two-step process, $L + M \rightarrow (LM)$, $(LM) + K \rightarrow LM + K$. Here, L and M are monomers, (LM) is the collision complex, and K is the third particle. The algorithm of this process is described below.

1. Velocities of the collision complex are calculated from the momentum conservation as

$$\bar{v}_{(LM)} = \frac{m_L \bar{v}_L + m_M \bar{v}_M}{m_{(LM)}} \quad (8)$$

2. The internal energy of the collision complex is calculated from energy conservation,

$$E_{(LM)}^{int} = E_L^{int} + E_M^{int} + \Delta E, \quad (9)$$

where $\Delta E = m_{(LM)} v_{(LM)}^2 - m_K v_L^2 - m_L v_M^2$.

3. The total energy of the collision complex - third particle pair is increased by the evaporation (or binding) energy E_{evap} ,

$$E^{total} = E_{(LM)-K}^{rel} + E_{(LM)}^{int} + E_K^{int} + E_{evap}. \quad (10)$$

Here, $E_{(LM)-K}^{rel}$ is the relative translation energy of the $(LM) - K$ collision. Evaporation energy is a function of cluster size, and the values used for Ar and H₂O are given in the following sections. Note that E_K^{rot} may be used instead of E_K^{int} , since the vibrational mode of third particles will barely be excited at the low temperatures at which homogeneous condensation usually occurs.

4. New energies $E_{(LM)-K}^{rel}$, $E_{(LM)}^{int}$, E_K^{int} are sampled using the Larsen-Borgnakke scheme⁴⁸ extended to multiple energy modes.³²

C. Elastic and inelastic reflective collisions of monomers and clusters

The interactions between monomers and clusters is one of the key processes that determine the nucleation rate. The reason for it is strong dependence of the evaporation rate on the cluster internal energy. Since the monomers are dominant in the flows considered here, the cluster internal energy is mostly governed by its relaxation through cluster-monomer collisions. In this work, a hard sphere model is assumed for cluster-monomer collisions, with the cluster diameter determined from Eqn. 7 for dimers, and for larger clusters from an empirical correlation used extensively in the past (see, for example, Ref. 12),

$$d = 2 \cdot (A \cdot i^{\frac{1}{3}} + B), \quad (11)$$

where A and B are species-dependent constants, and i is the number of monomers in the cluster. In this work, the values of A and B were 2.3×10^{-10} m and 3.4×10^{-10} m for argon, and 1.9×10^{-10} m and 2.4×10^{-10} m for water.

For the energy transfer between the relative translational and internal modes of the cluster and monomer, the Larsen-Borgnakke model is used, and a parameter Z is introduced that has a meaning of the internal energy relaxation number. The energy transfer between all energy modes of the cluster-monomer pair occurs with a probability Z^{-1} , and an elastic collision with no internal energy exchange occurs with the additional probability $1 - Z^{-1}$. A value of $Z = 6$ was used in the present calculations, that allows reasonable agreement of the DSMC rates for dimer nucleation and dissociation with rates available in the literature.

D. Sticking collisions of monomers and clusters

When a monomer collides with a cluster, sticking of the monomer to a cluster surface is possible, in addition to a reflective collision described in the previous section. For small clusters, monomer sticking is the main process that governs the evolution of the droplet size distribution.⁴⁴ An empirical dependence of the sticking probability on the species radius and mass, given in Ref. 49, is used in this work. This dependence reduces to

$$\epsilon = \frac{d_n^2}{d_n^2 + d_1^2} \left(\frac{m_n}{m_n + m_1} \right), \quad (12)$$

where indices n and 1 refer to the cluster and monomer, respectively.

The following algorithm is used to model sticking of a molecule to a cluster L to form a larger cluster K .

1. Calculate velocities of K as

$$\bar{v}_k = \frac{m_L \bar{v}_L + m_M \bar{v}_M}{m_k} \quad (13)$$

2. After velocities \bar{v}_K are assigned, the new internal energy is calculated

$$E_K^{int} = E_L^{int} + E_M^{int} - Q + \Delta E \quad (14)$$

Here,

$$\Delta E = -m_K \bar{v}_K^2 + m_L \bar{v}_L^2 + m_M \bar{v}_M^2$$

and $Q \equiv E_{evap}$ is the evaporation energy of one monomer off cluster K .

The only outcome for cluster-cluster collisions is assumed to be coalescence. The algorithm for cluster-cluster sticking collisions is similar to the monomer-cluster collision, with the exception of $Q = -Q_K + Q_L + Q_M$, where Q_i is the energy of vaporization of cluster i .

E. Evaporation rate and algorithm

Following Ref. 31, RRK theory is used to model the evaporation process. The evaporation rate k_e is calculated as

$$k_e = \nu N_s \left(\frac{E_{int} - E_{evap}}{E_{int}} \right)^{3n-7} \quad (15)$$

Here, n is the number of monomers in the cluster, ν is the vibration frequency, N_s is the number of surface atoms, and E_{int} is the cluster internal energy. For dimers, the exponent $3n - 7$ is replaced with 1. The number of surface atoms is n for $N < 5$, $n - 1$ for $4 < n < 7$, and $(36\pi)^{1/3}(n^{1/3} - 1)^2$ for $n > 6$. The vibration frequency was taken to be $2.68 \times 10^{12} \text{ s}^{-1}$ for water clusters, and 10^{12} s^{-1} for argon clusters. Since

$$\frac{dN_s}{dt} = -k_e N_s, \quad (16)$$

the time τ to the next evaporation event for a given cluster may be sampled from $\tau = -\ln \frac{R}{k_e}$. The algorithm used to model the evaporation process for a given cluster over a simulation timestep ΔT is as follows.

1. Set $t_{local} = 0$
2. Calculate k_e
3. Change $t_{local} = t_{local-1} - \ln(R)/k_e$
4. If $t_{local} > \Delta t$, exit.
5. Evaporate one monomer (see below).
6. If the remaining cluster is a monomer, exit. Else, go to Step 3.

F. Energy redistribution in evaporation

The following energy redistribution scheme is used to model the evaporation of a monomer M off a cluster K , with a smaller cluster L formed.

1. Decrease the internal energy of K by the evaporation energy E_{evap}

$$E_K^{int} = E_K^{int} - E_{evap} \quad (17)$$

2. Split cluster internal energy E_K^{int} between the relative translational energy E_{rel} and the internal energy of the M – L pair (the sum of the smaller cluster internal energy and the monomer internal energy), E_{int} using the Larsen-Borgnakke procedure.
3. Split energy E_{int} between the smaller cluster internal energy and the monomer internal energy using the Larsen-Borgnakke procedure.
4. Calculate new smaller cluster and monomer velocities using E_{rel} , keeping in mind that the center of mass of the new pair has the same velocity as the velocity of the original cluster.

G. Evaporation energy and the number of internal degrees of freedom

It is important to use reasonable values for the evaporation energy of a monomer off a cluster and the number of cluster internal degrees of freedom as a function of cluster size. The values of the evaporation energy were taken from Refs. 50,51 for water clusters and Ref. 52 for argon clusters. The number of cluster internal degrees of freedom is calculated from the expression for the average internal energy $\langle E \rangle$ of a cluster of a size n

$$\langle E \rangle = \frac{\xi^{int}}{2} kT = nC_v T - \frac{3}{2} kT$$

as

$$\xi^{int} = n \frac{2C_v}{k} - 3$$

where C_v is the cluster heat capacity. For water, the values of C_v were taken from Refs. 50,51, while for argon, they were assumed to approximate an expression $\xi^{int} = 2(3n - \eta)$, where η is 5 for $n = 2$ and 6 otherwise.⁵³ Both the heat capacity and evaporation energies are listed in Table G. For the cluster sizes larger than given below, the values for the maximum listed sizes are used.

Cluster size	H ₂ O E_{evap} , J	H ₂ O C_v , J/K	Ar E_{evap} , J	Ar C_v , J/K
2	4.919E-20	8.347E-23	0.989E-21	0.17E-22
3	6.329E-20	9.773E-23	1.978E-21	0.21E-22
4	1.021E-19	1.029E-22	2.967E-21	0.26E-22
5	1.122E-19	1.070E-22	3.84E-21	0.29E-22
6	1.009E-19	1.106E-22	4.48E-21	0.31E-22
7	7.210E-20	1.138E-22	5.92E-21	0.33E-22
8	6.889E-20	1.166E-22	4.70E-21	0.34E-22
9	6.729E-20	1.192E-22	6.08E-21	0.34E-22
10	6.569E-20	1.218E-22	6.13E-21	0.35E-22
11	6.409E-20	1.234E-22	6.24E-21	0.36E-22
12	6.409E-20	1.243E-22	6.64E-21	0.36E-22
13	6.409E-20	1.250E-22	5.76E-21	0.37E-22

Table 1. The water and argon cluster heat capacities and evaporation energies per monomer.

The first principle condensation model described here was implemented in the DSMC code SMILE.⁵⁴ The validation of the code through the comparison with theoretical and experimental results is presented below.

III. Thermal bath relaxation

Inelastic cross sections for monomer-monomer and monomer-cluster collision processes are necessary for detailed validation of a kinetic condensation model. These cross sections, generally functions of the energy states, both translational and internal, of pre- and post-collisional particles, are not available for most gas and temperature conditions of interest. Contrary to the energy dependent cross section, the integral temperature dependent rates for such collisions at conditions close to equilibrium are available in the literature. Therefore, one of the key indicators of the accuracy and reliability of a condensation model is its ability to produce

realistic rates of evaporation and nucleation at equilibrium. Although matching the rates generally does not guarantee correct behavior in nonequilibrium, it still is a necessary condition for a model to satisfy.

In this work, thermal bath relaxation of pure argon and pure water are examined at different temperature conditions, and the dimer formation rates for argon and equilibrium constants for the formation of dimers in argon and water are calculated and compared to the published results.⁵⁵⁻⁵⁷ In all thermal bath results, one million simulated particles were used, and the run proceeded until the steady state is reached, after which the results were sampled for 20 thousand timesteps. The number density was 5×10^{23} molec/m³ for argon and 2×10^{23} molec/m³ for water. The timestep of 2.5×10^{-11} s was selected so that the number of collisions per molecule is much smaller than unity, and the results are independent on the timestep.

The computed dimer formation rates k_{rec} for argon are presented in Fig. 1, where they are compared with the stable dimer formation rate of Ref. 55, where they were calculated using classical trajectories, and the following expression was proposed,

$$k_{rec} = 10.15T^{-0.278} \exp \{-0.0031T\}.$$

Generally, the present dimer formation rates are in reasonable agreement with the classical trajectory calculations, with the maximum difference approaching 20% for higher temperatures. Note that the computed rate has visibly smaller slope than that of Eqn. III. A number of factors could be affecting the slope, among them are the temperature dependence of the dimer stabilization probability and the heat capacity, that were not included in the present model, as well as the evaporation energy value and the after-reaction energy redistribution (recall that the Larsen-Borgnakke model was used for the energy redistribution).

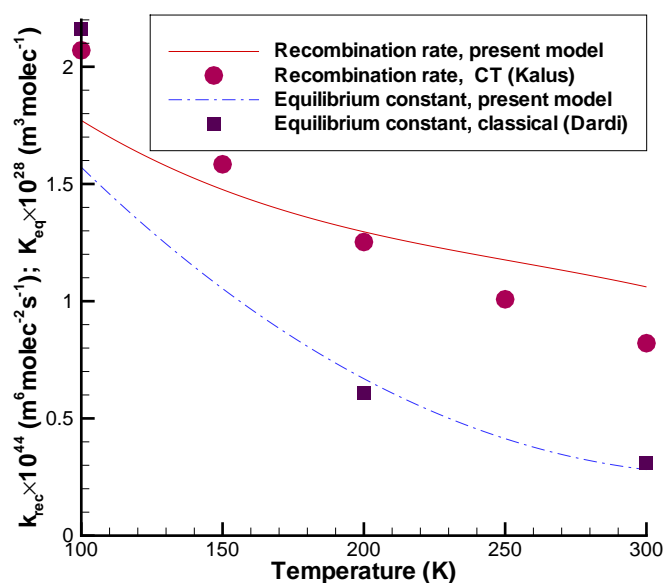


Figure 1. Argon dimer formation rate and equilibrium constant as functions of gas temperature.

The computed equilibrium constant, K_{eq} that is the ratio of the dimer dissociation to the dimer formation rate, is also given in Fig. 1. It is compared to the theoretical results of Ref. 56, where a number of approximate classical and quantum method are compared with exact numerical calculations. Note that while the results for different models and interaction potentials were found to be widely different, there was a good agreement between analogous quantum and classical calculations. Figure 1 shows that there is a very good agreement for temperatures of 200 K and higher, whereas for 100 K the present rate underpredicts that of Ref. 56. Similar to the dimer formation rates, the slope for the equilibrium constant obtained with the present model is smaller than the theoretical one; the reasons for this may be similar to those listed for the dimer formation rates.

An important factor that influences the magnitude of the equilibrium constant K_{eq} was found to be the probability of the energy transfer between the internal modes of a dimer and the translational modes in dimer-monomer collisions, Z^{-1} . This may be explained as follows. The dimers are formed after three-body collisions, and typically have internal energies smaller than the evaporation energy after those collisions. In argon, the evaporation energy for a dimer is relatively small compared to the typical total collision energy for all temperatures under consideration ($E_{evap}/k \approx 70$ K). That means that most of the dimers will have their internal energy in excess of the evaporation energy just after one or two collisions with monomers. The lifetime of the dimers whose internal energy is larger than the evaporation energy is very short, on the order of a picosecond. This results in the dimer-monomer energy transfer being the main process that leads to quick dimer dissociation. Note that the value of Z has negligible impact on the dimer formation rates, and only the evaporation rates are affected. As a result, in the range of temperatures considered in this work, the equilibrium constant for argon was found to be nearly proportional to Z^{-1} . For example, at 200 K $K_{eq} = 0.11 \times 10^{-26}$ m³/molec when $Z = 1$ is used, versus $K_{eq} = 0.66 \times 10^{-26}$ m³/molec for the baseline case of $Z = 6$.

The Z dependence of the equilibrium constant is quite different for water molecule condensation. In this case, the evaporation energy of a dimer is much larger than the translational energy of colliding molecules and dimers (the reduced evaporation energy $E_{evap}/k \approx 3,500$ K, compared to gas temperatures on the order of 300 K). The high value of the evaporation energy results in longer lifetimes of dimers, since much more collisions are necessary to transfer enough energy from the translational modes to the internal modes of a dimer. The dependence of K_{eq} on Z is therefore much weaker for water than for argon. In a 250 K thermal bath, K_{eq} decreases from 0.605×10^{-26} m³/molec to 0.343×10^{-26} m³/molec when Z decreases from 6 to 1. Note that since the number of internal degrees of a dimer is large, typically about 22, the average reduced energy per mode is ~ 160 K. This results in the energy in dimer-monomer collisions being mostly transferred from the translational modes to the dimer internal modes for the gas temperatures higher than 160 K (which is the case in most of the flow scenarios considered in this work).

Comparison of the equilibrium constant obtained with the present model, with the theoretical results of Ref. 57, where a flexible potential energy surface fitted to spectroscopical data was used, is shown in Fig. 2. Note that there are a number of theoretical predictions of the equilibrium rate of water dimerization, and they differ by at least a factor of three in the range of temperatures considered in this work. Reference 57 was chosen for comparison as the most sophisticated and one of the most recent ones. The following expression, adapted from Ref. 57, is used here,

$$K_{eq} = 6.5202 \times 10^{-32} T \exp \{1851.09/T - 5.10485 \times 10^{-3} T\}.$$

There is a very good agreement for gas temperatures above 270 K. For lower temperatures, the results obtained with the present model start to deviate. The difference reaches 60% at 200 K, with the present results being smaller. This general trend of underprediction at lower temperatures is similar to that of argon bath.

IV. Dimer mole fraction correlation in argon orifice expansion

An additional key measure of the accuracy and reliability of a condensation model is the terminal dimer mole fraction from a sonic orifice, where a semi-empirical correlation is available,⁴³ based on a large number of experimental data points. In this work, argon expansion from a sonic orifice is modeled at several different source temperatures and number densities. The computational domain consists of a section of a plenum 2.5 mm in radius and 2.5 mm in length, along with an expansion region that is 2.5 mm in radius and 7 mm in length. The DSMC runs use on average about 10 million simulated molecules and 2 million collision cells. The terminal dimer mole fractions are recorded, averaged, and compared to published results.⁴³

Generally, the terminal dimer mole fraction occurs when the expanding gas is at low enough densities to be nearly collisionless, and the cluster mole fraction reaches an equilibrium value. As seen in Fig. 3, this occurs well within the computational domain. 4 mm downstream of the orifice, number density in a typical case drops by 2 orders of magnitude. Near the outflow boundary, the number density decreases by yet another order of magnitude, and the gas mean free path in that region is on the order of the orifice diameter. Note that the figure is stretched in the radial direction to allow better detail.

Cluster mole fraction reached a terminal value in all of the cases considered in this work, as seen in Fig. 4 (left). Note that both higher number densities and lower temperatures increase both source and terminal

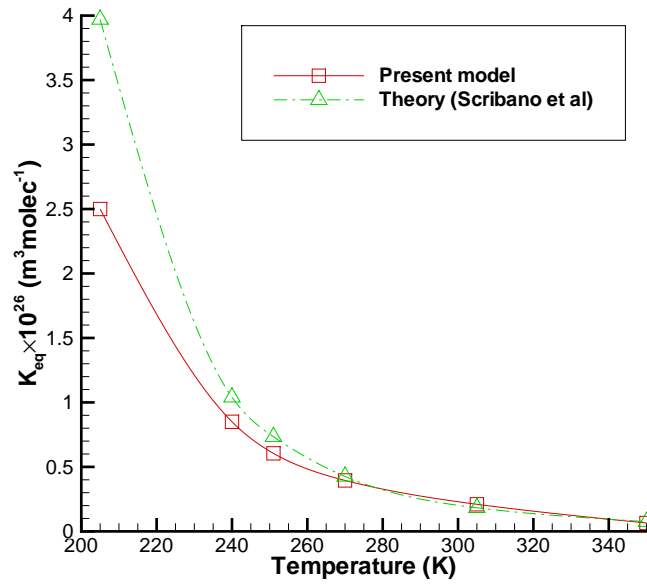


Figure 2. Water equilibrium constant as a function of gas temperature.

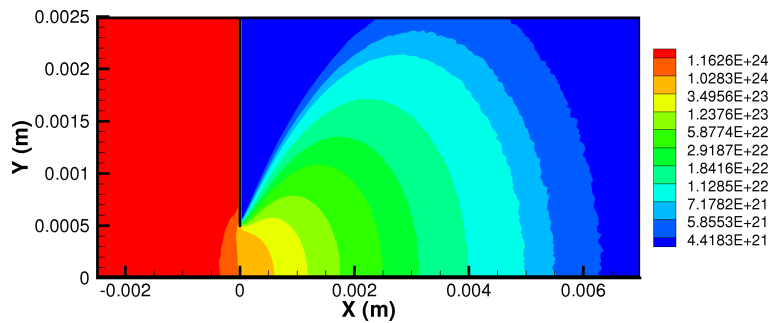


Figure 3. Number density flowfield from a sonic orifice with a source temperature and number density of 200 K and $1.2 \times 10^{24} \text{ m}^{-3}$, respectively.

cluster mole fractions. It is also worth noting that the mole fractions in the plenum are in good agreement with the equilibrium constants calculated in Ref. 56. This figure is also indicative of mole fraction of dimers along the plume, as the clusters are mainly dimers with a small number of trimers at most points in the plume.

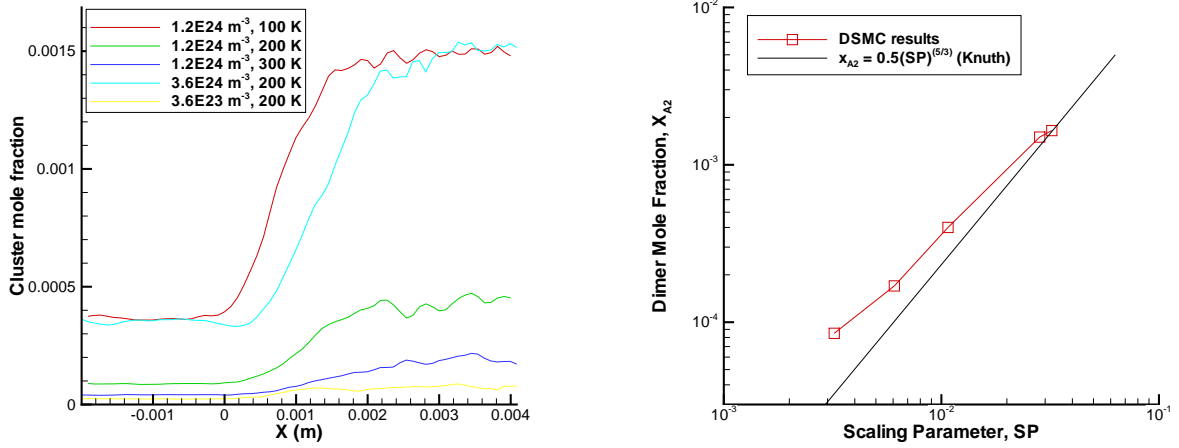


Figure 4. Cluster mole fractions along the axis for all cases considered, left, and average terminal dimer mole fraction along the axis as a function of scaling parameter SP .

Finally, the average terminal dimer mole fraction is shown in Fig. 4 (right) as a function of a scaling parameter SP . SP is given in Ref. 43 as: $SP = n_0 \sigma^3 \left(\frac{\epsilon}{kT_0}\right)^{\frac{7}{5}} \left(\frac{d^*}{\sigma}\right)^{\frac{2}{5}}$. The results of this work are shown compared to an empirical expression derived in Ref. 43, $x_{A_2} = 0.5 \times \left(n_0 \sigma^3 \left(\frac{\epsilon}{kT_0}\right)^{\frac{7}{5}} \left(\frac{d^*}{\sigma}\right)^{\frac{2}{5}}\right)^{\frac{5}{3}}$. The DSMC results are in reasonably good agreements with the results of Ref. 43, although a noticeable divergence from correlation values occurs at low values of the scaling parameter, which correspond to low number densities or high temperatures. Note that the empirical correlation underpredicted the data in that region.

V. Water cluster size distribution in nozzle flows

The last part of the validation and numerical analysis of the presented condensation model is focused on the nucleation and evolution of small water clusters in a small conical nozzle. The study was prompted by the availability of quality experimental data⁴⁴ on terminal size distribution of water clusters in the range of flow conditions where the Knudsen number was relatively large so that the computational cost of using the DSMC method is not prohibitive (although still rather high). The results are presented for the nozzle geometry of Ref. 44. The nozzle is a conical nozzle with a 41° opening angle, a total length of 2 mm, and a throat diameter of $50 \mu\text{m}$. The smallest stagnation pressure considered in Ref. 44, 1.577 bar, is used in this work, with the corresponding stagnation temperature of 495 K. Two constant temperatures of the nozzle surface were considered in the present computations to study the effect of surface temperature distribution, the baseline 495 K (stagnation temperature) and 300 K (room temperature). Since the background pressure effect in the experiment is believed to be small,⁵⁸ the flow expansion into the vacuum is modeled.

The axisymmetric capability of SMILE was used, with the total number of simulated molecules and collision cells about 80 million and 10 million, respectively. A uniform 400×100 grid was used for sampling of macroparameters and distribution functions. The Larsen-Borgnakke model with temperature-dependent relaxation numbers was used for energy transfer in monomer-monomer collisions, and the reflection of particles on the nozzle surface was assumed to be fully diffuse. Uniform inflow conditions were imposed at the nozzle throat, calculated from the isentropic flow relations at a constant specific heat ratio of 1.4.

The first set of results presented here shows the effect of the condensation on the gas flow inside the nozzle and in the plume near field. The gas translational temperature and axial velocity is shown in Fig. 5 for two cases, the baseline condensation model and the condensation turned off. The results show that the condensation practically does not change the flow parameters inside the boundary layer. This is expected, since the temperature in the boundary layer is higher than in the coreflow, and the nucleation near the

surface are not likely. Near the centerline, though, the condensation, being an exothermic process, results in a significant heat release. The temperature in that region visibly increases, with the maximum change of over 20 K. The higher temperature for the condensing flow, accompanied by fast translational relaxation, causes an increase in the axial velocity in the coreflow of about 30 m/s. The velocity change inside the boundary layer is negligibly small.

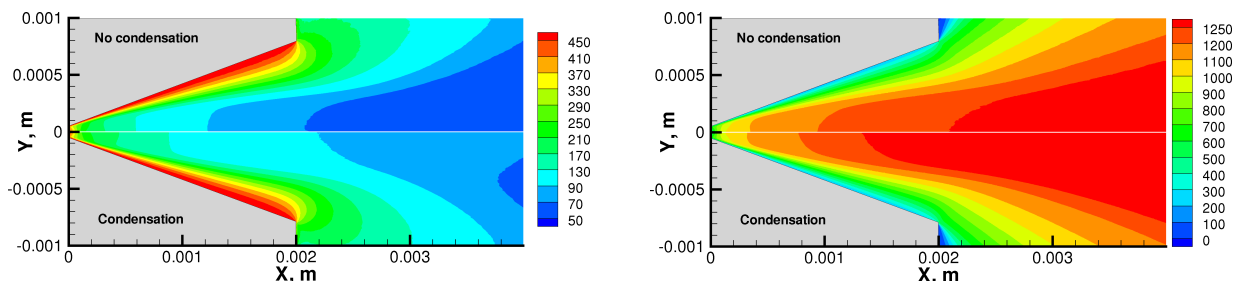


Figure 5. Impact of the condensation on the water translational temperature (K), left, and axial velocity (m/s), right.

Consider now the effect of the nozzle surface temperature in the condensing water flow, illustrated in Fig. 6. Generally, a higher wall temperature should result in thicker boundary layer, which is consistent with the temperature distributions shown in Fig. 6 (left). The influence of the wall temperature on the coreflow is negligible in the first quarter of the nozzle, and still relatively small further downstream. The temperature in the plume coreflow is only about 7 K higher for 495 K case. It is interesting that there is practically no impact of the wall temperature on the condensation process in the nozzle core flow, as the water cluster mole fraction given in Fig. 6 (right) illustrates. Although the region where the condensation occurs is larger for the colder wall case, the mole fraction profiles along the nozzle axis for 300 K and 495 K are within the statistical accuracy of the calculations. Generally, the cluster concentration increases rapidly in the first 100 μm from the nozzle throat, and reaches its maximum of about 1.5% at $\sim 200\mu\text{m}$. Then, the evaporation and cluster coalescence result in some decrease of the cluster concentration.

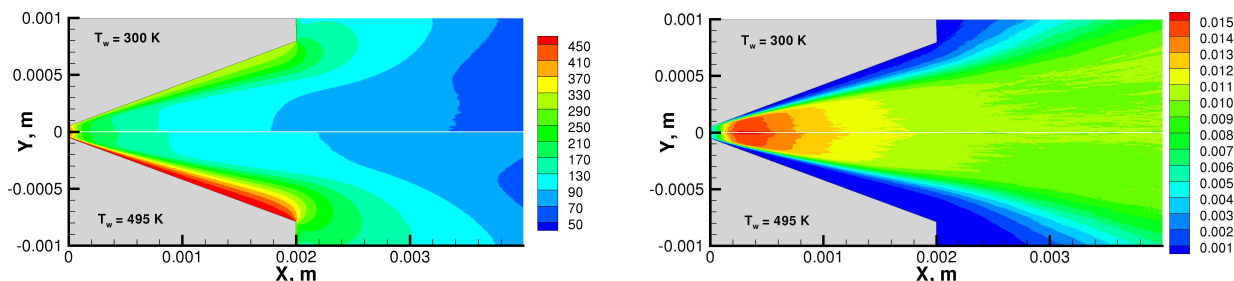


Figure 6. Impact of the nozzle surface temperature on the water translational temperature (K), left, and cluster mole fraction, right.

The computations conducted for a higher stagnation pressure of 5.177 bar have shown relatively little effect of pressure on both gas temperatures and number of clusters in the flow (see Fig. 7). The boundary layer thickness decreases with increasing pressure, whereas the temperatures in the coreflow are practically the same in the first quarter of the nozzle. Further downstream, in part due to the condensation heat release, the temperature in the coreflow is a few degrees higher for the larger pressure case. The cluster mole fraction is somewhat higher for 2.177 bar, but generally the increase is less than ten percent. Again, there is a clear maximum in the cluster mole fraction, and its location does not change with pressure.

In addition to a small increase in the number of clusters with stagnation pressure, the average cluster size also increases with higher pressure. The average cluster size as a function of the axial distance along the nozzle axis, calculated as the mean value of monomers in a cluster, is presented in Fig. 8. The number of clusters larger than dimers is larger for 2.177 bar case at any point in the flow, and the relative difference increases with the distance from the throat. Due to larger number of collisions, it takes longer for the higher pressure case to reach the terminal size distribution, that appears to be further downstream than the 4 mm distance from the throat computed in this work.

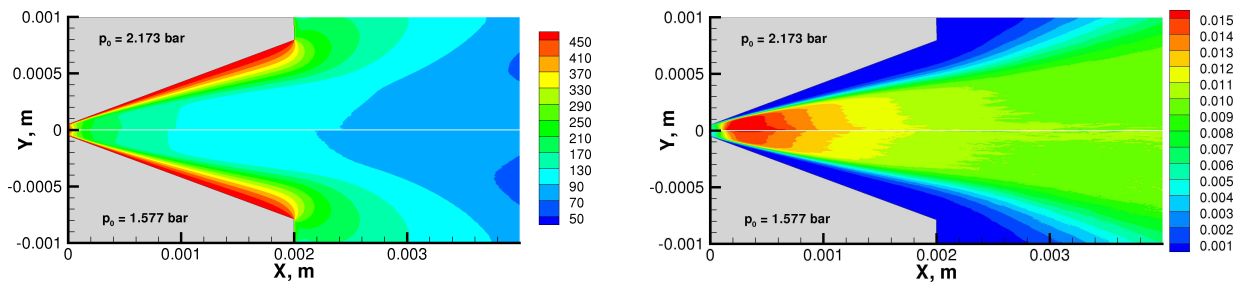


Figure 7. Impact of the stagnation pressure on the water translational temperature (K), left, and cluster mole fraction, right.

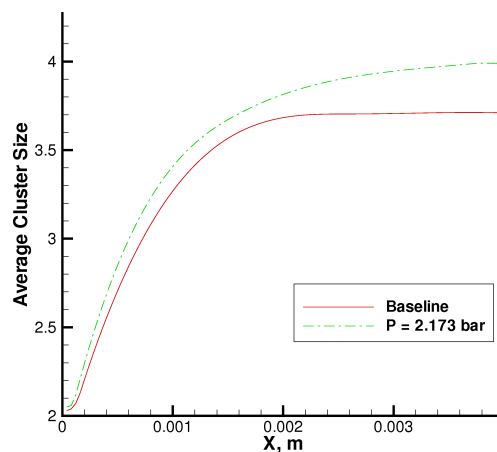


Figure 8. Average cluster size along the nozzle axis for two different pressures.

Following the analysis of the impact of different physical flow parameters presented above, a sensitivity study has been conducted to estimate possible effect of parameters of the model. In addition to the baseline computation, the cases with a larger $Z = 1$ (compared to the baseline of $Z = 6$) and smaller values of the cluster evaporation energies and cluster heat capacities (both decreased by 20%) were used. Note that these are relatively large changes that are believed to represent the limiting cases for the corresponding parameters. The cluster mole fractions for these four cases are presented in Fig. 9. Note that the clusters represent a trace species with typical mole fractions on the order of one percent, and statistical scatter is visible for them (the species weights were not used here in order to avoid any potential energy non-conservation issues that they may cause). The cluster mole fraction profiles were therefore smoothed using a B-spline approximation routine in SMILE. It is interesting to note that the mole fraction terminal value is only weakly sensitive to the varied parameters. It is about 1% for all cases under consideration. The transient behavior in the first half of the nozzle significantly differs for these cases, though. The decrease in the heat capacity is in effect the decrease in the number of cluster internal degrees of freedom. Smaller number of internal degrees of freedom of a cluster means that when the Larsen-Borgnakke routine is used for energy redistribution (the energy is split proportionally to the number of degrees of freedom), it will take more collisions to raise the cluster's internal energy to the values exceeding the evaporation threshold. As a result, more clusters are present in the flow. When the cluster evaporation energy values are reduced, smaller number of clusters are observed in the flow, since they become easier to evaporate. The cluster internal energy relaxation number has relatively small effect on cluster populations.

The above arguments for the impact of different parameters of the model are still applicable when the average cluster size is examined. Only the change in Z has relatively minor effect in this case. To the contrary, the decrease in the heat capacity significantly increases, and in evaporation energy, increases, the average cluster size. Note also that changing all three parameters seems to increase the relaxation length as compared to the baseline case, where the cluster fraction and size distribution come to their terminal values soon after the nozzle exit.

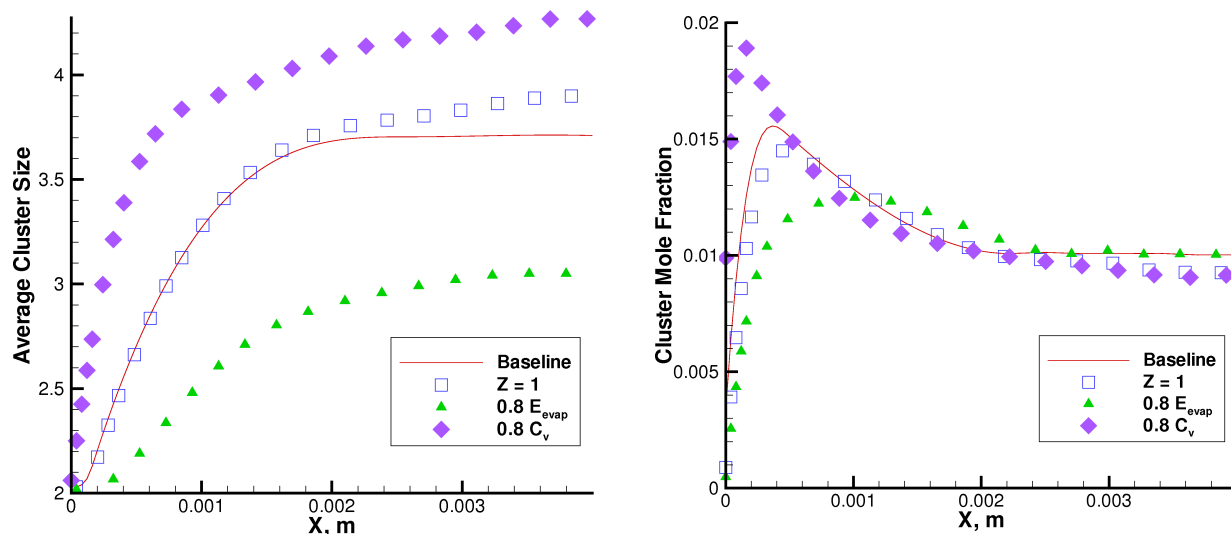


Figure 9. Cluster mole fraction, right, and average cluster size, left, along the nozzle axis for different parameters of the condensation model.

Comparison of the terminal size distribution obtained for the baseline model, with experimental results^{44, 59} is shown in Fig. 10. In the experiments, the dimers were below the detection threshold, the trimer population may be somewhat affected by that threshold, and all larger clusters are believed to be recorded without significant distortions. For side-by-side comparison, the experimental size distribution was normalized so that it has the same fraction of clusters larger than dimers as in the computation. The results show that while there is a reasonable agreement between the numerical modeling and measurements, there is a maximum for the cluster sizes of 5 and 6 observed in the computations, that were not recorded experimentally. The reason for this maximum is the corresponding maximum in the evaporation energies for these cluster sizes (see Table G). It is possible that more accurate or general values of evaporation energies (only one water molecule orientation was considered in Ref. 50) have to be used to obtain better agreement with the data.

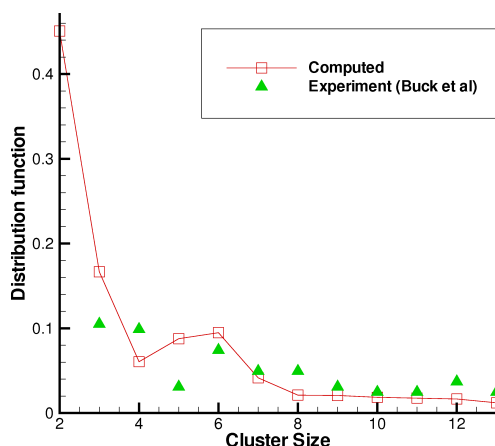


Figure 10. Comparison of the computed size distribution with experimental data of Ref. 44.

VI. Conclusions

A first-principle condensation model applicable for the DSMC method is constructed. It was validated through comparison with available theoretical and experimental data on condensation rates in a thermal bath, dimer mole fractions in orifice expansions, and cluster size distributions in nozzle flows. The model is

based on a DSMC model of recombination reaction for the collision based dimer formation, and the RRK model for the cluster evaporation. Cluster growth is modeled through cluster-monomer and cluster-cluster collisions. The energy transfer in these collisions is calculated using the extended Larsen-Borgnakke principle. An important parameter that controls the rate of internal energy transfer in cluster-monomer collisions is analyzed, and the sensitivity of evaporation rates to this parameter is shown.

Two gases are considered in this work, argon and water. For the thermal bath relaxation, the present model was found to capture the equilibrium constants for water and argon and nucleation rates for argon fairly well in the considered range of temperatures from 100 K to 350 K. The computed slope was somewhat smaller than theoretical for lower temperatures, which may be attributed to the accuracy of used physical and numerical parameters of the condensation model. Comparison of terminal mole fractions in a sonic orifice expansion dimer with the available semi-empirical correlations showed that the new model agrees reasonably with the correlations, overpredicting the latter by about a factor of two for lower pressures and higher temperatures.

Sensitivity of the clusterization to the cluster internal energy relaxation number, cluster evaporation energies, and heat capacities, has been examined and shown for water expansion through a conical nozzle. Additional studies are necessary to further refine the utilized values of the above parameters. Comparison of the cluster size distribution with the available experimental data has been conducted, and reasonable agreement between the computations and the experiments have been shown.

VII. Acknowledgments

The water nozzle flow part of this work would be impossible without the help of Prof. Udo Buck. The authors are extremely thankful for his support and patience in explaining experimental setup and data, and providing additional data on cluster size distributions. The work was supported in part by the Propulsion Directorate of the Air Force Research Laboratory at Edwards Air Force Base California.

References

- ¹F. Abraham, *Homogeneous Nucleation Theory: The Pretransition Theory of Vapor Condensation*. New York: Academic Press, 1974.
- ²A. Zettlemoyer, *Nucleation Phenomena*. New York: Wiley, 1977.
- ³A. Itkin and E. Kolesnichenko, *Microscopic Theory of Condensation in Gases and Plasma*. Singapore: World Scientific, 1997.
- ⁴P. ten Wolde and D. Frenkel, "Computer simulation study of gas-liquid nucleation in a Lennard-Jones system," *J. Chem. Phys.*, vol. 109, p. 9901, 1998.
- ⁵H. Hettema and J. McFeaters, "The direct Monte Carlo method applied to the homogeneous nucleation problem," *J. Chem. Phys.*, vol. 105, p. 2816, 1996.
- ⁶S. Girshick, "Comment on: Self-consistency correction to homogeneous nucleation theory," *J. Chem. Phys.*, vol. 94, p. 826, 1991.
- ⁷J. E. McDonald, "Homogeneous nucleation of vapor condensation II. Kinetic aspects," *Am. J. Phys.*, vol. 31, p. 31, 1963.
- ⁸B. S. Lukyanchuk, W. Marine, S. I. Anisimov, and G. A. Simakina, "Condensation of vapor and nanoclusters formation within the vapor plume, produced by ns-laser ablation of Si, Ge and C," *Proceedings of SPIE*, vol. 3, no. 618, p. 434, 1999.
- ⁹H. Haberland, "Experimental methods," in *Clusters of Atoms and Molecules*, edited by H. Haberland (Springer, Berlin), p. 207, 1994.
- ¹⁰M. A. Ratner, "Kinetics of cluster growth in expanding rare-gas jet," *Low Temp. Phys.* Translated from Russian Journal *Fiz. Nizk. Temp.*, 25, 367, 1999., vol. 25, p. 266, 1999.
- ¹¹Y. P. Raizer, "Condensation of a cloud of vaporized matter expanding in vacuum," *Soviet Physics JETP*, vol. 37, p. 1229, 1959.
- ¹²J. Zhong, M. Zeifman, S. Gimelshein, and D. Levin, "Direct Simulation Monte Carlo Modeling of Homogenous Condensation in Supersonic Plumes," *AIAA Journal*, 2005, Vol. 43, No. 8, pp. 1784-1796.
- ¹³J. Zhong, D. A. Levin, and M. I. Zeifman, "Modeling of argon condensation in free jet expansions with the DSMC method," *Proc. XXIV Int. Symp. on Rarefied Gas Dynamics*, ed. M Capitelli, AIP Conference Proceedings, Vol. 762, New York, 2005, pp. 391-395.
- ¹⁴W. Williams and J. Lewis, "Summary report for the CONSET program at AEDC," Arnold Engineering Development Center, no. AEDC-TR-80-16, 1980.
- ¹⁵Ohkubo et al [Ohkubo, M. Kuwata, B. Lukyanchuk, and T. Yabe, "Numerical analysis of nanocluster formation within ns-laser ablation plume," *Appl. Phys.*, vol. A 77, p. 271, 2003.
- ¹⁶M. Sharaf and R. Dobbins, "A comparison of measured nucleation rates with the predictions of several theories of homogeneous nucleation," *J. Chem. Phys.*, vol. 77, p. 1517, 1982. and references therein.
- ¹⁷M.I. Zeifman, J. Zhong, D.A. Levin, "Applicability of the homogeneous nucleation theory to the condensation in free gas

expansions," Proc. XXIV Int. Symp. on Rarefied Gas Dynamics, ed. M Capitelli, AIP Conference Proceedings, Vol. 762, New York, 2005, pp. 391-395.

¹⁸D. Willis, B. Hamel, and J. Lin, "Development of the distribution function on the centerline of a free jet expansion," Phys. Fluids, vol. 15, p. 573, 1972.

¹⁹R. Cattolica, F. Robben, L. Talbot, and D. Willis, "Translational nonequilibrium in free jet expansions," Phys. Fluids, vol. 17, p. 1793, 1974.

²⁰G. Bird, "Transition regime behavior of supersonic beam skimmers," Phys. Fluids, vol. 19, p. 1486, 1976.

²¹G. Schenter, S. Kathmann, and B. Garrett, "Variational transition state theory of vapor phase nucleation," J. Chem. Phys., vol. 110, p. 7951, 1999.

²²G. K. Schenter, S. M. Kathmann, and B. C. Garrett, "Dynamical nucleation theory: A new approach to vapor-liquid nucleation," Phys. Rev. Lett., vol. 82, p. 3484, 1999.

²³B. Senger, P. Schaaf, D. S. Corti, R. Bowles, J. C. Voegel, and H. Reiss, "A molecular theory of the homogeneous nucleation rate. I. Formulation and fundamental issues," J. Chem. Phys., vol. 110, p. 6421, 1999.

²⁴B. Senger, P. Schaaf, D. S. Corti, R. Bowles, D. Pointu, J. C. Voegel, and H. Reiss, "A molecular theory of the homogeneous nucleation rate. II. Application to argon vapor," J. Chem. Phys., vol. 110, p. 6438, 1999.

²⁵H. Hettema and J. McFeaters, "The direct Monte Carlo method applied to the homogeneous nucleation problem," J. Chem. Phys., vol. 105, p. 2816, 1996.

²⁶J. Soler, N. Garcia, O. Echt, K. Sattler, and E. Recknagel, "Microcluster growth: transition from successive monomer addition to coagulation," Phys. Rev. Lett., vol. 49, p. 1857, 1982.

²⁷M. Valerica, M. Casey, J. Goodisman, , and J. Chaiken, "Application of fractals and kinetic equations to cluster formation," J. Chem. Phys., vol. 98, p. 4610, 1993.

²⁸S. Toxvaerd, "Molecular-dynamics simulation of homogeneous nucleation in the vapor phase," J. Chem. Phys., vol. 115, p. 8913, 2001.

²⁹T. Ikeshoji, B. Hafskjold, Y. Hashi, and Y. Kawazoe, "Molecular dynamics simulation for the cluster formation process of Lennard-Jones particles: Magic numbers and characteristic features," J. Chem. Phys., vol. 105, p. 5126, 1996.

³⁰M.I. Zeifman, J. Zhong, D.A. Levin, A Hybrid MD-DSMC Approach to Direct Simulation of Condensation in Supersonic Jets, AIAA Paper 2004-2586.

³¹M. Zeifman, B. J. Garrison, , and L. V. Zhigilei, "Combined molecular dynamics – direct simulation Monte Carlo computational simulation of laser ablation plume evolution," J. Appl. Phys., vol. 92, p. 2181, 2002.

³²G. A. Bird, Molecular Gas Dynamics and the Direct Simulation of Gas Flows. Oxford: Clarendon Press, 1994.

³³H. Mizuseki, Y. Jin, Y. Kawazoe, and L. T. Wille, "Growth processes of magnetic clusters studied by direct simulation Monte Carlo method," J. Appl. Phys., vol. 87, p. 6561, 2000.

³⁴H. Mizuseki, K. Hongo, Y. Kawazoe, and L. Wille, "Multiscale simulation of cluster growth and deposition processes by hybrid model based on direct simulation Monte Carlo method," Comp. Mat. Sci, vol. 24, p. 88, 2002.

³⁵J. Zhong, M. Zeifman, D. Levin, Kinetic model of condensation in a free expanding jet, J. Thermophysics and heat transfer, 2006, Vol. 20, No. 1, pp. 41-51.

³⁶A. Gallagher-Rogers, J. Zhong, D.A. Levin, "Simulation of Homogeneous Ethanol Condensation in Supersonic Nozzle Flows Using DSMC," AIAA Paper 2007-4159.

³⁷J. Zhong and D. Levin, "Development of a Kinetic Nucleation Model for a Free-Expanding Argon Condensation Flow," AIAA Journal, 2007, Vol. 45, No. 4, pp. 902-911,

³⁸B. Briehl and H. Urbassek, "Monte Carlo simulation of growth and decay processes in a cluster aggregation source," J. Vac. Sci. Tech., A, Vol. 17, No. 1, p. 256, 1999.

³⁹S. Gratiy, J. Zhong, D.A. Levin, "Numerical Simulation of Argon Condensation with a Full Kinetic Approach in a Free-Expanding Jet," AIAA Paper 2006-3598.

⁴⁰M. F. Jarrold, in Clusters of Atoms and Molecules, edited by H. Haberland Springer, Berlin, 1994, p. 163.

⁴¹R.D. Levine, Molecular reaction dynamics, Cambridge University Press, 2005.

⁴²S.F. Gimelshein, M.S. Ivanov, "Simulation of Chemically Reacting Gas Flow Using Majorant Frequency Scheme of DSMC," Proc. XVII Intern. Symp. on Rarefied Gas Dynamics. Vancouver, Canada. 1994. Vol.159. pp. 218-233.

⁴³E.L. Knuth, "Size correlations for clusters produced in free-jet expansions," J. Chem. Phys., **101** (21) 1997, pp. 9125-9132.

⁴⁴C. Bobbert, S. Schutte, C. Steinbach, U. Buck, "Fragmentation and reliable size distributions of large ammonia and water clusters," Eur. Phys. J. D **19** pp. 183-192, 2002.

⁴⁵D.L. Bunker, "Mechanisms of atomic recombination reactions," J. Chem. Physics, 1959, Vol. 32, No. 4, pp. 1001-1005.

⁴⁶M.S. Ivanov and S.V. Rogasinsky, "Analysis of numerical techniques of the direct simulation Monte Carlo method in the rarefied gas dynamics," Sov. J. Numer. Anal. Math. Modelling **2** (6), 1988, pp. 453-465.

⁴⁷G.A. Bird, "Monte-Carlo simulation in an engineering context," In *Rarefied Gas Dynamics*, ed. S Fisher, Progress in Astronautics and Aeronautics, 1981, vol. 74, pp. 239-255.

⁴⁸C. Borgnakke and P.S. Larsen, "Statistical collision model for Monte Carlo simulation of polyatomic gas mixture," J. Comp. Phys., 1975, Vol. 18, pp. 405-420.

⁴⁹J.F. Crifo, Water clusters in the coma of Comet Halley and their effect on the gas density, temperature, and velocity, ICARUS, **84**, 1990, pp. 416-446.

⁵⁰S.V. Drozdov and A.A. Vostrikov, "Structural features and energy of small water clusters," Tech. Phys. Let., **26** (2), 2000, pp. 397-399.

⁵¹A.A. Vostrikov, S.V. Drozdov, V.S. Rudnev, L.I. Kurkina, "Molecular dynamics study of neutral and charged water clusters," Computational Materials Science, **35**, 2006, pp. 254-260.

⁵²R.L. Johnston, Atomic and molecular clusters. Taylor and Francis, New York 2002.

- ⁵³S.A. Losev, S.O. Macheret, B.V. Potapkin, G.G. Chernyi, Physical and chemical processes and gas dynamics: cross sections and rate constants. Progress in Astronautics and Aeronautics, 196, AIAA, 2002.
- ⁵⁴M.S. Ivanov, G.N. Markelov, S.F. Gimelshein, "Statistical simulation of the transition between regular and Mach reflection in steady flows," Computers and Mathematics with Applications, **35** (1-2), 1998, pp. 113-126.
- ⁵⁵R. Kalus, "Formation of argon dimers in ternary monomer collisions," J. Chem. Physics, **109** (19), 1998, pp. 8289-8294.
- ⁵⁶P.S. Dardi, J.S. Dahler, "Equilibrium constants for the formation of van der Waals dimers: Calculations, for Ar-Ar and Mg-Mg," J. Chem. Phys, **93** (5), 1990, pp. 3562-3572.
- ⁵⁷Y. Scribano, N. Goldman, R.J. Saykally, C. Leforestier, "Water dimers in the atmosphere III: equilibrium constant from a flexible potential," J. Phys. Chem. A, **110** (16), 2006, pp. 5411-5419.
- ⁵⁸S. Schütte, U. Buck, "Strong fragmentation of large rare gas clusters by high energy electron impact," Int. J. Mass Spec., **220**, 2002, pp. 183-192.
- ⁵⁹U. Buck, Private communication, 2009.